Plenary and invited lectures

SOME PROPERTIES OF VOLTERRA OPERATOR PENCILS

TSEDENBAYAR DASHDONDOG

DEPARTMENT OF MATHEMATICS, UNIVERSITY OF SCIENCE AND TECHNOLOGY, MONGOLIA
E-mail address: tsdnbr@must.edu.mn

ABSTRACT. We intend to present new methods of constructing power-bounded operators (related to the Volterra operator and Laguerre polynomials) with care of the behaviour of the differences of the consecutive power's in order to understand the way of achieving the Ritt condition. An analogy between the properties of the Volterra operator pencils (operator norm, numerical range, numerical radius) will be observed. Most of the results and problems come from my joint works with Yuri Lyubich.

EMBEDDED SYSTEM DESIGN IN SMART SYSTEM INTEGRATION: FROM OPEN SOURCE HARDWARE TO OPEN SOURCE SCIENCE

MANFRED GLESNER

TECHNISCHE UNIVERSITÄT DARMSTADT, FACULTY OF ELECTRICAL ENGINEERING AND INFORMATION TECHNOLOGY, GERMANY
E-mail address: glesner@mes.tu-darmstadt.de

ABSTRACT. According to the executive summaries of the GOSH-community hardware forms a vital part of the scientific experimental process and the current supply chain limits access and impedes creativity and customization through high mark-ups and proprietary designs. The Gathering for Open Science Hardware (GOSH) is a diverse, global community working to enhance the sharing of open, scientific technologies. Open source hardware addresses part of this problem through sharing open designs, which often take advantage of modern digital fabrication techniques. Expanding the reach of this approach within academic research, citizen science and education has potential to increase access to experimental tools and ease their customization and reuse while lowering costs. In the DIY-communities a growing number of people around the world are developing and using open source hardware in the context of the wider movement for Open Science, a trend is referred in proposals of the world-wide acting Open Science Hardware (OScH) community. However, in Europe such a movement is only slowly making progress. In the paper we discuss the status of the Open-Science Hardware approach to develop an open science hardware ecosystem which will play an important role for futuresmart system designs in the engineering community.

SHORT PAPER VERSION

Smart or intelligent system is a new technology term that will be found in many applications in our daily life and industries in the future for examples in energy management, medical applications and healthcare management, industrial automation and automotive. Based on its technological term, smart systems should have capabilities to solve very complex problems, including taking over human cognitive functions. Due to the exponential increase of world energy demand, in which between 2010 and 2030 is estimated to be 45%, energy management will be one of the most urgent topics of the century and a significant driver for the evolution of semiconductors and electronics products. The important issues in the energy management are efficiency and reliability. Those requirements initiate the movement of power technology trend from traditional into smart grids concept. Cybersecurity and control systems for instance will be important topics for future smart grid systems. In medical applications and healthcare management, smart products are mainly dedicated to improve the quality of health treatments and rehabilitations. The key components of the products are sensors (biomedical sensors). They should be miniaturized, which is enabled by using Micro-Electro-Mechanical System (MEMS) technology, in order to minimize the physical effect on the biologic system. The key factor of the smart systems is new inventions in the fields of nanotechnology, advanced materials, biotechnology, photonic technology and nanoelectronics. The innovation of efficient computing algorithms should be a challenging

issue to implement the nanoelectronic products. The integration of the nanoelectronic products into smart systems should consider both arts and cost aspect. Therefore, the miniaturization of smart products, which is affected by efficient computing algorithms and nano-scale technologies, will be an interesting feature for end-users on market.
In the talk we discuss especially the strategic importance of Open-Source-Hardware (=OSHW) Design Strategies which have recently received much attention. Different popular Open-Source-Embedded platforms are available on the market today under $100 costs. The Open-Source-Hardware-Association defines the term OSHW as follows:

"Open source hardware is hardware whose design is made publicly available so that anyone can study, modify, distribute, make, and sell the design or hardware based on that design. The hardware's source, the design from which it is made, is available in the preferred format for making modifications to it. Ideally, open source hardware uses readily-available components and materials, standard processes, open infrastructure, unrestricted content, and open-source design tools to maximize the ability of individuals to make and use hardware. Open source hardware gives people the freedom to control their technology while sharing knowledge and encouraging commerce through the open exchange of designs." World-wide we see an explosion in the development of a new infrastructure for the design of complex electronic systems.

In the meantime boards with enhanced features are on the market: Google (Mountain View, CA) has announced new versions of its do-it-yourself (DIY) artificial intelligence (AI) kits. With his Adafruit company Limor Fried is offering to the "Maker-Community" all the necessary hardware and software to build up complex embedded electronics. Also new fabrication facilities for small-volume electronics boards are built up on the market. There is a Hackaday-Community offering on their website free designs in the spirit of the Open Source Community. The best designs win prices on their annual Hackaday Super Conference.

CATALYTIC CONVERSION OF CO_2 TO FUEL

YANG, YANHUI

INSTITUTE OF ADVANCED SYNTHESIS, NANJING TECH UNIVERSITY, NANJING
E-mail address: yhyang@njtech.edu.cn

In the global attempt to reduce carbon footprint, the chemical and petrochemical industry faces the problem to replace the currently used fossil feedstock with renewable resources, reduce energy consumption and to intensify and integrate the processes to be more carbon efficient. In all three issues, catalysis will be the key to a successful transformation. Knowledge-based development and implementation of catalytic technology will help to process the novel feedstock, reduce the energy required for maintaining the desired process and improve the carbon efficiency of the targeted synthesis routes. In this seminar, two examples will be discussed to illustrate our efforts in the last year in CO_2 utilization.

The catalytic hydrogenation of CO_2 under atmospheric pressure is a hot topic in CO_2 utilization in which methanation and reverse water-gas shift (RWGS) serve two competing parallel pathways. Novel Ni-W-Mg mixed oxide catalysts (NiWMgOx) were prepared by homogeneous precipitation and attempted for the methanation of CO_2. Adding W remarkably promoted the activity with improved stability, anti-CO-poisoning ability and resistance against coke formation compared to the undoped NiMgOx catalyst. The superior reactivity of monodentate formate towards hydrogenation than that of bidentate formate species was identified by DRIFTS analysis and the formation of more active monodentate formate species was indisputably facilitated by W additives, leading to the greatly enhanced catalytic activity. H_2-TPR and CO_2-TPD characterization showed that doping W increased the number of stable CO_2 adsorption sites and helped in anchoring the Ni sites as a result of strengthened Ni-Mg interaction, both of which were responsible for the enhanced CO_2 methanation activity and the improved resistance against sintering.

The control mechanism of catalytic selectivity and structure-activity relation at atomic scale need further understanding. It has been suggested that the dispersion state and the size of metallic particles play a crucial role in determining CO_2 conversion and selectivity as well as stability. However, these studies have not considered the possible effect of interface sites between metal and oxide support in selective hydrogenation of CO_2. In this work, three structural configurations of monolayer, periphery and nanocluster in Ru/Al_2O_3 catalysts were obtained by control of Ru weight loadings, confirmed by the characterization results of the extended X-ray absorption fine structure, H_2-O_2 titration and diffuse reflectance infrared Fourier transform spectroscopy of CO adsorption. The kinetic data reveal the dependence of reaction rates for CO and CH_4 formation with different apparent activation energies on the Ru surface structures. Theoretical calculations of Ru_9/Al_2O_3 and Ru_{35}/Al_2O_3 models demonstrate that monolayer Ru sites favor the RWGS route

Key words and phrases. CO_2, catalytic conversion
† Corresponding author. Yang, Yanhui

with a relatively low energy barrier for both CO_2 activation and CO formation steps, while Ru nanoclusters prefer methanation route energetically. Moreover, the combination of theoretical calculations and experimental isotope-exchange measurements suggests that the interfacial O species in Ru-Al_2O_3 interfaces act a critical role in CO_2 activation via exchanging with O atom in feeding CO2 and incorporating into the final hydrogenation products.

DECAY RATE OF GLOBAL SOLUTIONS TO THE SCHÖDINGER EQUATION WITH CUBIC DISSIPATIVE NONLINEARITY

NAOYASU KITA†

†FACULTY OF ADVANCED SCIENCE AND TECHNOLOGY, KUMAMOTO UNIVERSITY, JAPAN
E-mail address: nkita@kumamoto-u.ac.jp

ABSTRACT. We consider the optimality of decay estimate of solutions to the initial value problem of 1D Schrödinger equations containing cubic dissipative nonlinearity $\lambda|u|^2u$, where $\mathrm{Im}\lambda < 0$. Our aim is to obtain the fact that, if the L^∞-norm of a solution admits a decay rate more rapid than the designated one and then it must be a trivial solution.

1. INTRODUCTION AND MAIN RESULT

We consider the Cauchy problem of 1D-nonlinear Schrödinger equation:

$$\begin{cases} i\partial_t u = -\dfrac{1}{2}\partial_x^2 u + \lambda |u|^2 u, \\ u(0,x) = u_0(x), \end{cases} \tag{1.1}$$

where $t \in [0,\infty)$, $x \in R$, $\lambda = \lambda_1 + i\lambda_2$ $(\lambda_1, \lambda_2 \in R)$ and $\lambda_2 < 0$. By considering the associated nonlinear ODE: $i\partial_t u = \lambda|u|^2u$, we see that $\partial_t|u|^2 = \lambda_2|u|^4 \le 0$. Therefore the condition $\lambda_2 < 0$ implies the dissipation. The equation as in (1.1) arises in the nonlinear fiber engineering. According to Chapter 11 in [1] or physical manuscript [2], here is a complex Ginzburg-Landau equation:

$$i\frac{\partial U}{\partial \xi} - \frac{1}{2}(s+id)\frac{\partial^2 U}{\partial \tau^2} + N^2 |U|^2 U = \frac{i}{2}(\mu - \mu_2 |U|^2)U$$

where U denotes the dimension-less amplitude of electric field propagating through an optical fiber, ξ the position along the optical fiber, τ the time-variable expressing the oscillation of the electric field, s, d, N, μ and μ_2 denotes the scales of dispersion, diffusion, nonlinear Kerr effect, amplification and nonlinear dissipation, respectively. Therefore the equation (1.1) corresponds to the special case of this model, in which $s < 0$, $d = 0$ and $\mu = 0$. We want to treat this model as an evolution equation, and so replace the variables ξ and τ by t and x respectively, following mathematical convention.

It is well known that the large-time asymptotic behavior of global solutions to (1.1) is different from that of solutions to the corresponding free equation (see [3]). It suggests that the nonlinearity keeps affecting the solution for a long time. There are some works on the small initial value problem of (1.1) (see e.g., [5]), in which the L^∞-decay estimate of global solutions, i.e.,

$$\| u(t) \|_{L^\infty} \le Ct^{-1/2}(\log t)^{-1/2} \tag{1.2}$$

was proved.

Key words and phrases. grant systems, Boolean vector

The large initial value problem of (1.1) together with strong dissipative condition: $|\lambda_1| \le \sqrt{3}|\lambda_2|$ was considered in [4], where the L^∞-decay estimate as in (1.2) was proved. Our purpose in this paper is to investigate the optimality of decay rate in (1.2). In other words, we are going to prove that, if a solution decays more rapidly than (1.2) shows, then the initial data u_0 must be 0. Our main result is

Theorem 1.1. *Let $\lambda_2 < 0$. We also assume that, for $u_0 \in H^1 \cap H^{0,1}$, the solution u to (1.1) is well-posed in $C([0,\infty); H^1 \cap H^{0,1}) \cap C^1([0,\infty); H^{-1})$. If the solution admits a decay estimate like*

$$\| u(t) \|_{L^\infty} = o(t^{-1/2}(\log t)^{-1/2}) \tag{1.3}$$

as $t \to \infty$, then $u_0 = 0$.

Remark. Theorem1.1 suggests that the solutions, which was obtained in [4], [5] and indicate the decay rate as in (1.2), are optimal. We can no more refine the decay rate of solutions to (1.1), except for $u_0 = 0$.

Throughout this paper, we employ the following notation. For $q \in [1,\infty)$, the L^q denotes the set of measurable function f satisfying $\|f\|_{L^q} := \int_R |f(x)|^q dx < \infty$. The L^∞ denotes the set of measurable function f satisfying $\|f\|_{L^\infty} := \text{ess.sup}|f(x)| < \infty$.
The Sobolev space H^1 stands for the set of integrable function f such that $f \in L^2$ and the derivative in distribution sense $\partial_x f \in L^2$. The norm of H^1 is given by $\|f\|_{H^1} := \|f\|_{L^2} + \|\partial_x f\|_{L^2}$. The dual space of H^1 is denoted by H^{-1}.

2. PRELIMINARY

This section is devoted to the preliminary for the proof of Theorem 1.1. We first consider the L^2-decay estimate of $u(t)$. It will be applied in order to derive $u(T) = 0$ for some large $T > 0$.

Proposition 2.1.[L^2-decay] *Assume the same assumptions as in Theorem* (1.1). *Then, for any $\sigma > 0$, there exist some $C_\sigma > 0$ and $T_\sigma > 0$ such that*

$$\| u(t) \|_{L^2} = C_\sigma (\log t)^{-1/3+\sigma} \tag{2.1}$$

holds for $t \in [T_\sigma, \infty)$.

When we prove Proposition 2.1, the lemma below will be taken into account.

Lemma 2.2. *Assume the same assumptions as in Theorem (1.1). Then, for any $\varepsilon > 0$, there exist some $C_\varepsilon > 0$ and $T_\varepsilon > 0$ such that*

$$\| \partial_x u(t) \|_{L^2} + \| Ju(t) \|_{L^2} \le C_\varepsilon (\log t)^\varepsilon$$

holds for $t \in [T_\varepsilon, \infty)$, where $J = x - it\partial_x$ (the generator of Galilean transform).

Proof of Lemma 2.2. For the rigorous proof, the technique of cut-off and mollification is required. But we shall proceed in formal way. Multiply $\overline{\partial_x u}$ on both hand sides of

(1.1) after applying ∂_x. Then we have

$$\begin{aligned}\partial_t \| \partial_x u(t) \|_{L^2}^2 &= 2\,\mathrm{Im}\Big\{\lambda \int \partial_x (|u(t,x)|^2 u(t,x))\,\overline{\partial_x u(t,x)}\,dx\Big\} \\ &= 2\lambda_2 \int |u(t,x)|^2 |\partial_x u(t,x)|^2\,dx + \mathrm{Im}\Big\{\lambda \int u(t,x)^2\,(\overline{\partial_x u(t,x)})^2\,dx\Big\} \\ &\le 2\lambda_2 \int |u(t,x)|^2 |\partial_x u(t,x)|^2\,dx + |\lambda| \int |u(t,x)|^2 |\partial_x u(t,x)|^2\,dx \\ &\le C \| u(t) \|_{L^\infty}^2 \| \partial_x u(t) \|_{L^2}^2 . \end{aligned} \tag{2.2}$$

In virtue of (1.3), we see that, for any $\varepsilon > 0$, there exists some $T_\varepsilon > 0$ such that

$$\partial_t \| \partial_x u(t) \|_{L^2}^2 \le 2\varepsilon t^{-1} (\log t)^{-1} \| \partial_x u(t) \|_{L^2}^2 . \tag{2.3}$$

holds for $t \in [T_\varepsilon, \infty)$. Applying Gronwall's inequality, we have

$$\begin{aligned}\| \partial_x u(t) \|_{L^2} &\le (\log t)^{\varepsilon} (\log T_\varepsilon)^{-\varepsilon} \| \partial_x u(T_\varepsilon) \|_{L^2} \\ &\le C_\varepsilon (\log t)^{\varepsilon} .\end{aligned}$$

The similar inequality holds for Ju by noting that J and $\mathrm{i}\partial_t + \frac{1}{2}\partial_x^2$ commute and by applying

$$\mathrm{J}(|u|^2 u) = 2|u|^2 \mathrm{J}u - u^2 \overline{\mathrm{J}u}. \qquad \square$$

Proof of Proposition 2.1. For the solution u satisfying the assumption of Theorem 1.1, we have

$$\partial_t \| u(t) \|_{L^2}^2 = 2\lambda_2 \| u(t) \|_{L^4}^4 . \tag{2.4}$$

Applying Hölder's inequality: $\|u\|_{L^4}^4 \|u\|_{L^1}^2 \ge \|u\|_{L^2}^6$ to the right hand side of (2.4), we see that

$$\partial_t \| u(t) \|_{L^2}^2 \le 2\lambda_2 \frac{\| u(t) \|_{L^2}^6}{\| u(t) \|_{L^1}^2} . \tag{2.5}$$

The L^1-norm in (2.5) is estimated by (scale-invariant) Schwarz' inequality, i.e.,

$$\begin{aligned}\| u(t) \|_{L^1} &\le C \| u(t) \|_{L^2}^{1/2} \| xu(t) \|_{L^2}^{1/2} \\ &\le C \| u(t) \|_{L^2}^{1/2} \| Ju(t) + it\partial_x u(t) \|_{L^2}^{1/2} ,\end{aligned}$$

where we used $x = J + it\partial_x$ in the last inequality. Applying this estimate to (2.5), we see that

$$\partial_t \| u(t) \|_{L^2}^2 \le -C \frac{\| u(t) \|_{L^2}^5}{\| Ju(t) \|_{L^2} + t \| \partial_x u(t) \|_{L^2}} .$$

By Lemma 2.2, it follows that, for $t \in [T_\varepsilon, \infty)$,

$$\partial_t \| u(t) \|_{L^2}^2 \le -Ct^{-1}(\log t)^{-\varepsilon} \| u(t) \|_{L^2}^5 \tag{2.6}$$

Solving the differential inequality (2.6) with $\varepsilon \in (0, 1/2)$, we have, for $t \in [T', \infty)$ with $T' > 0$ sufficiently large,

$$\| u(t) \|_{L^2} \le -C(\log t)^{-1/3+\varepsilon/3}.$$

Taking $\sigma = \varepsilon/3$ and $T' = T_\sigma$, we obtain Proposition 2.1. □

3. Proof of Theorem 1.1

We are now at the position to prove Theorem 1.1.

Proof of Theorem 1.1. For the solution u satisfying the assumption of Theorem 1.1, we have

$$\begin{aligned} \partial_t \| u(t) \|_{L^2}^2 &= 2\lambda_2 \| u(t) \|_{L^4}^4 \\ &\ge 2\lambda_2 \| u(t) \|_{L^\infty}^2 \| u(t) \|_{L^2}^2 \end{aligned} \tag{3.1}$$

By the decay-assumption (1.3), we see that, for any $\varepsilon > 0$,

$$\partial_t \| u(t) \|_{L^2}^2 \ge -2\varepsilon t^{-1}(\log t)^{-1} \| u(t) \|_{L^2}^2 \tag{3.2}$$

holds if t is sufficiently large. By applying Gronwall's inequality to (3.2), we have, for $t > T$,

$$(\log t)^{\varepsilon} \| u(t) \|_{L^2} \ge (\log T)^{\varepsilon} \| u(T) \|_{L^2} \tag{3.3}$$

We here apply Proposition 2.1 to the right hand side of (3.3). Then we see that, for sufficiently large $T > 0$,

$$C_\sigma (\log t)^{-(1/3)+\sigma+\varepsilon} \ge (\log T)^{\varepsilon} \| u(T) \|_{L^2}. \tag{3.4}$$

Take $\varepsilon > 0$ and $\sigma > 0$ sufficiently small so that the left hand side of (1.4) tends to 0 as $t \to \infty$. Then we see that $u(T) = 0$. Solving (1.1) backward in time, we see that $u_0 = 0$ The proof of Theorem 1.1 is complete.

Acknowledgments

This work is basically supported by JSPS Grant-in-Aid for Scientific Research (C) No.17K05305. The author would also like to express his appreciation to Research Institute for Mathematical Sciences, an International Joint Usage/Research Center located in Kyoto University, for giving him fruitful opportunities to participate in the joint research activity titled "Reaction Diffusion Equations and Nonlinear Dispersive Equations" held on 25-27 of September, 2017 and the workshop titled "Qualitative Theory on ODEs and its Applications to Mathematical Modeling" held on 12-14 of November, 2018. He could receive valuable comments and suggestions from the participants.

REFERENCES

[1] G. P. Agrawal, *Nonlinear fiber optics*, Academic Press, Inc. (1995).

[2] G. P. Agrawal, Effect of two-photon absorption on the amplification of ultrashort optical pulses, Phys. Rev. E, **48**(1993), 2316-2318.

[3] J. Barab, *Nonexistence of asymptotically free solutions for a nonlinear Schrödinger equation*, J. Math. Phy., **25**(1984), 3270-3273.

[4] N. Kita and A. Shimomura, *Large time behavior of solutions to Schrödinger equations with a dissipati ve nonlinearity for arbitrarily large initial data*, J. Math. Soc. Japan, **61**(2009), 39-64.

[5] A. Shimomura, *Asymptotic behavior of solutions to Schrödinger equations with dissipative nonlineariti es*, Comm. Partial Differential Equations, **31**(2006), 1407-1423.

RESOURCE EXPLORATION AND ENVIRONMENTAL MONITORING WITH THE NEW AIRBORNE PLATFORM D-MTUC

HERD RAINER[1,2], HOLST JON[3]

[1]BRANDENBURG UNIVERSITY OF TECHNOLOGY (BTU), COTTBUS, GERMANY
[2]GERMAN-MONGOLIAN INSTITUTE FOR RESOURCES AND TECHNOLOGY (GMIT), NALAIKH, MONGOLIA
[3]GEODUSTER TECHNOLOGIES CC, KNYSNA, REPUBLIC OF SOUTH AFRICA

E-mail address: herd@b-tu.de

ABSTRACT. D-MTUC is the identification of a recently developed airborne investigation system. The lack of regional investigation data in a lot of regions, an increasing demand on spatial underground information, increasing restrictions to access private property and the lack of affordable commercially operated systems for projects with small budgets were main reasons beside others for the Chair Raw Material and Natural Resource Management of Brandenburg University of Technology Cottbus, Germany to develop, construct and assemble a multi-sensor airborne investigation system based on a full composite ultra-light aircraft. As a base or platform for the system, the model 'VIRUS SW 100' of the manufacturer Pipistrel, Slovenia has been chosen after an evaluation process and set of flight and "noise" tests. Due to the requirements of the chair concerning demount ability, sufficient payload, modification potential and cost effectiveness competitors like helicopter and drone had to be sorted out. Prior to the final fabrication of D-MTUC all possible and necessary modifications have been discussed with the engineers of the manufacturer resulting in an "low noise" aircraft built especially for the demands of a multi sensor investigation platform.
The actual geoscientific instrumentation comprehends a CsI-y-spectrometer, 2 K-magnetometer and a VLF-EM-receiver with the option of further sensor installations. The actual configuration enables the system to operate at low speed and low altitude for mineral exploration, geological mapping, detection of freshwater resources and brines and different environmental monitoring missions.

Key words and phrases. Airborne investigation, airborne monitoring, airborne geophysics

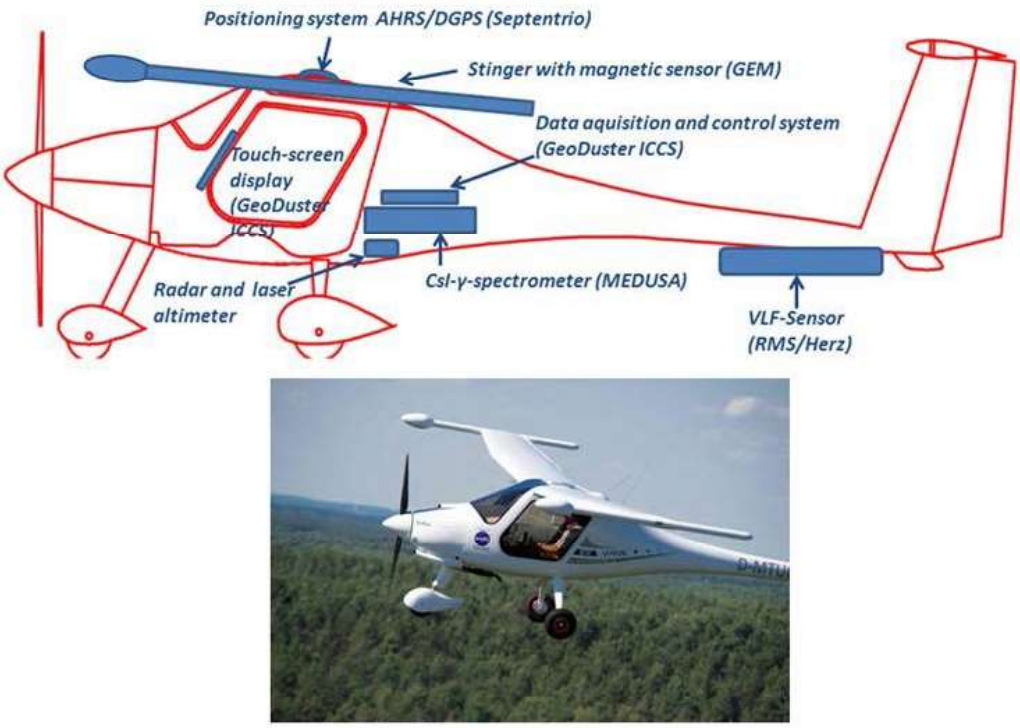

FIG. 1: The ultra-light airborne investigation system D-MTUC with actual sensor equipment

REFERENCES

[1] Herd, R. & Holst, J. (2015): *D-MTUC, an airborne investigation system based on a full composite ultra-light aircraft. In: Meyer, U. & Miensopust, M. (Eds.): Airborne Geophysics-New technologies in Hardware and Interpretation,* Deutsche Geophysikalische Gesellschaft Sonderband II/2015, p. 10-13, Potsdam, ISSN-Nr. 0947-1944

CHARACTERIZATION OF NARIIN SUKHAIT COAL AND IT'S PYROLYSIS PRODUCTS.

B.PUREVSUREN[1], A.ARIUNAA[1], S.JARGALMAA[1], B.BATULZII[1], B.AVID[1]

[1]INSTITUTE OF CHEMISTRY AND CHEMICAL TECHNOLOGY, MAS, ULAANBAATAR-51, MONGOLIA.

ABSTRACT. Present investigation on Nariin sukhait coal focused on characterization of the initial coal and it's hard and liquid products after pyrolysis. First of all on the basis of proximate, ultimate and petrographic analysis of Nariin sukhait coal have been confirmed that the Nariin sukhait coal is bituminouse high rank coal with G mark. The thermal degradation process of Nariin sukhait coal was investigated by thermogravimetric analyzer and first time determined the thermal stability of the coal sample by determination of thermal indices such as $T_{5\%}$ -425,3°C; $T_{15\%}$ -498,6°C; $T_{25\%}$ -620,0 °C from the TG curve, which are the characteristics higher thermal stability. The pyrolysis of Nariin sukhait coal carried out at different heating temperatures and determined the yields of obtained hard, liquid and gas products. A most suitable heating temperature was chosen 700°C, in which the yield of condensed liquid product -3,6% (tar) was higher. The yield of all liquid (tar and pyrolysis water) and gas products (16,0%) shows that there was a thermal decomposition of the coal organic mass with lower degree of conversion. The highest yield of hard residue after pyrolysis shows that the coal organic mass of Nariin sukhait coal has higher thermal stability and it is more suitable for coking and activation. The determined chemical composition of pyrolysis tar of Nariin sukhait coal in group organic compounds by chemical analysis show that the tar consists mostly neutral oils with highest content-85,0%, asphalteines -13,6%, organic acids and phenolic compounds are with lower content, organic bases and asphalteins are with lowest content. The pyrolysis tar of Nariin sukhait coal also was distilled at room temperature and obtained 4 fractions with different boiling temperature ranges including yellow colored light fraction (18-180 °C), 2 yellow-green colored middle fractions (180-250 °C and 250-320 °C) and black colored heavy fraction (330 > °C). The SEM image of initial coal sample Nariin sukhait has compact solid pieces. The SEM image of carbonized and activated coal sample shows a porosity structure with meso and macro pores in comparison with that of initial coal sample. The solubility in hexane, benzene and dichloromethane and chemical composition of the pyrolysis tar of Nariin sukhait coal investigated by silicagel chromatograpy and chemical composition of the each separated fractions determined by GC/MS analysis. All 41 compounds identified from all registered 100 peaks of soluble in hexane, 35 compounds identified from all registered 50 peaks of soluble in benzene, and 19 compounds identified from all registered 91 peaks of soluble in dichloromethane in the pyrolysis tar of Nariin sukhait coal.

1. INTRODUCTION

Mongolia is among the 10 coal rich countries in the world with the 175 billion tones of geologically estimated coal resources including high quality bituminous coking coals, subbituminous coals and lignite brown coals [1,2].

Key words and phrases. Nariin sukhait coal, pyrolysis, hard residue, tar.

† Corresponding author. B.Purevsuren

The Nariin sukhait coal deposit is one of the largest high quality bituminous coal in the Southern economic region of Mongolia and the estimated geologically coal resources is 125,5 million tones. The Nariin sukhait coal deposit locates in the territory of Gurvantes village of South Gobi province and is a open-cast mine, which belongs to the MAK Company [3]. First time the coal of Nariin sukhait deposit was a subject for more detailed characterization and pyrolysis in our laboratory.

2. EXPERIMENTAL

The analytical coal samples of Nariin sukhait deposit were prepared for analysis according to ASTM D 2797. The main technical characteristics such as proximate and ultimate analysis were performed according to Mongolian National Standards MNS 656-79 (moisture content), MNS 652-79 (ash yield), MNS 654-79 (volatile matter yield), MNS 669-87 (gross calorific value) and MNS 895-79 (sulphur content).

For the determination of mineral content in Nariin sukhait coal have been obtained completely burned ashes of coals during slowly and continuously burning in furnace at 200-950 °C. The content of mineral elements in coal samples and their oxides have been determined by using of X-ray fluorescence spectrometry.

Petrographic analysis was performed on polished particulate mounts following recommendations by the International Committee for Coal and Organic petrology [4].

Vitrinite reflectance was measured using an Axio Imager M2m microscope (Zeiss, Germany) and fossil software (Hilgers, Germany) on 50 individual vitrinite macerals in random mode conducted according to ASTM D 2798. In addition, a modification of ASTM D 2799 using fluorescence microscopy was employed for rapid qualitative information on maturity and organofacies.Vitrinite particles were characterized with higher reflectivity than autochthonous vitrinite.

Usually, only the vitrinite population with the lowest reflectance values is measured and reported. Maceral group analysis was performed using the same microscope and software by point counting of 500 individual macerals.The petrographic analysis, vitrinite reflectance and maceral group composition are important for the investigation of the microcomponent of the coal organic mass and determination of the coal type, and quality which are important characteristics for the thermal decomposition of coal organic mass.

The small-scale pyrolysis experiments of coal samples were performed in a laboratory quarts retort (tube) which could contain air dried and powdered to a particle size < 0,2 mm 1 g- of coal sample. The retort was placed in a horizontal electric tube furnace with a maximum heating temperature of 950 °C. A chrome-alumel thermocouple was immersed in the tube furnace to measure the actual heating temperature.The pyrolysis experiments have been carried out at different heating temperatures 200 -700 °C with constant heating rate 20 °C/min. First of all the quarts retort with coal sample was heated for example to 600 °C with heating rate 20 °C/min. and kept at 600 °C for 80 min. The retort was connected with a thermostable glass tube heated also in a tube furnace at 80 °C for collecting of tars and this tube is also connected with a air-cooled glass vessel for collecting of pyrolysis water. The glass vessel for pyrolysis water is also connected with a thin glass tube for non-condensable gases. The yields of pyrolysis products including solid residue (coal char), tar (condensed liquid product) and pyrolysis water determined by weighing, and the yield of gases by differences.

The prepapative-scale pyrolysis experiments of coal sample was performed in a laboratory vertical cylindrical retort made by stainless steel which could contain 1000 g. of sample. The retort was placed in an electric furnace (model SNOL) with a maximum temperature of 950 °C. A chrome-alumel thermocouple was immersed in the *coal bed* to measure the actual heating temperature and an equipment for temperature control (potentiometer). The retort was connected with a air-cooled iron tube and water-cooled laboratory glass condenser and a collection vessel for the condensed of liquid product (tar and pyrolysis water). The non-condensable gases after water-cooled condenser were left the system through a thin glass tube. The yields of products including hard residue (char), tar and pyrolysis water determined by weighing in %, and the yield of gases by difference.

The liquid condensed by product of coal pyrolysis consists from tar and pyrolysis water. They form an unmixed two layers and can be separated easily by separating glass funnel. The upper layer is tar (viscous liquid) with black-brown color and unpleasant smell. The bottom layer is pyrolysis water (no viscous liquid) with bad smell and brown color. The final cleaning of tar from the pyrolysis water usually use thermally treated $CaCl_2$ by mixing and separating (filtering or centrifuging).

The Fourier transform infrared spectroscopy (FTIR) spectra of the samples were obtained on a Interspec 200-X series of FTIR spectrometers with PIKE Diffusion IR accessories using a KBr disc containing 1% finely ground samples. All the spectra were measured in the frequency range of 4000 to 400 cm-1, and 32 scans were taken per sample.

First of all organic bases and organic acids were removed from the pyrolysis tar of Shivee-Ovoo coal and so purified tar is called as a ''neutral oil''.

The column chromatography conditions neutral oil as follow:

- Small glass column: 5.0 ml
- Sample of tar 0.2g. for each solvent
- Used organic solvents (pure for chromatography): hexane, toluene and methylenchloride : methanol (1:1 mass ratio) -20,0 ml from each solvent.
- Used sorbent: activated silicagel 4.0g.

The column chromatography carried out for obtaining of the soluble in hexane (H), toluene (T) and methylenechloride and methanol (M) fractions of the neutral oil. These fractions were used for GC/MS analysis.

The conditions of GC/MS analysis of each fractions are:

-The analytical sample of each fraction: 1 microliter of each fraction in 1 ml of each solvent.

-The sample of of GC/MS analysis: 1 microliter from each analytical sample.

-Used apparatus: Agilent 7890A Agilent 5975C GCMS system and capillary column J&W DB-5,30mx, 0.25mm I.D. 0.25µm (122-5032).

-Carrier gas: He

-Mass range: 50-550.

- Starting temperature of furnace: 100 °C.

-Heating temperature and time: 220 °C, 46 min.

3. RESULTS AND DISCUSSION

The results of proximate and ultimate analysis of coal samples from Nariin sukhait deposit are shown in Table 1.

TABLE 1. Proximate and ultimate analyses of Nariin sukhait coal

Sample	Proximate analysis, %				Ultimate analysis, %					
	Moisture, W^a	Ash, A^d	Volatile matter, V^{daf}	Caloric value, Q^{daf}, kcal/kg	Carbon, C^{daf}	Hydro-gen, H^{daf}	Sulfur total, S_t	Nitrogen, N^{daf}	Oxygen and others, $(+O)^{daf}$	C/H
Nariin sukhait coal	1,0	15,8	36,9	7685	84,9	4,4	1,6	0,5	10,2	0,7

The results of proximate and ultimate analysis in Table 1 for example the content of volatile matter, the ratio of H/C, carbon content indicate that coal from Nariin sukhait deposit is a high rank G mark ( ) stone coal. The contents of total sulfur and nitrogen are not higher and not so dangerous for the environment.

The content of different type of sulfur of Nariin sukhait coal determined by chemical analysis and the results are given in Table 2.

TABLE 2. The content of different type of sulfur of Nariin sukhait coal.

Sample	The content of different type of sulfur, (%)			
	Total, S_t^d	Pirit, S_p^d	Sulphate, S_{so4}^d	Organic, S_o^d
Nariin sukhait coal	1,6	0,31	0,29	1,0

The content of different type of sulfur of Nariin sukhait coal in Table 2 show that the most part of total sulfur is organic type of sulfur and as mentioned above the Nariin sukhait coal has lower content of total sulfur.

To characterize the organic matter of the Nariin sukhait coal has been analyzed by IR analysis and the IR spectra is shown in Figure 1.

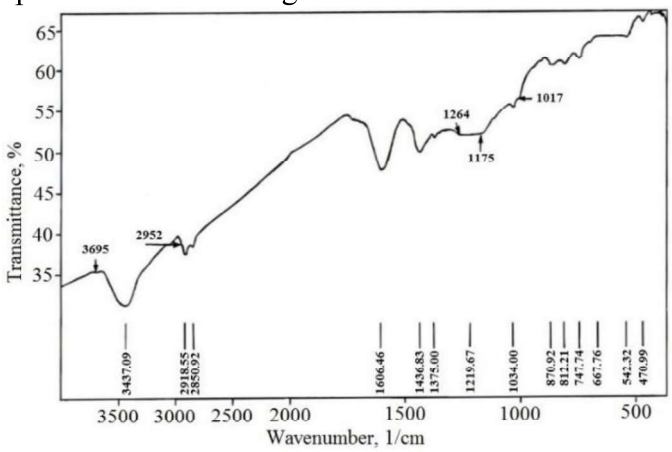

Figure 1. The IR spectra of coal from Nariin sukhait deposit.

In the IR spectra (Figure 1) of Nariin sukhait coal there are several week absorption bands for -CH aromatic group at 698, 752, 800 cm^{-1} and for aliphatic -CH; $-CH_2$ and –

CH_3 groups with middle intensity at 1249 cm-^{1} and a sharp bands with higher intensity at 2854-2923 cm^{-1}. And and also a strong absorption bands for >C=O groups at 1600 cm^{-1}, week bands for -O- groups at 1400 cm^{-1} and for C-O- groups at 1000, 1050 cm^{-1}. A unsharp and strong band for -OH and -NH groups at 3400 cm-^{1}. Therefore the coal organic mass of Nariin sukhait coal consist mainly aliphatic, aromatic and aromatic-aliphatic structures with above mentioned groups inside.

Petrographic analysis was carried out on polished coal samples using the same microscope and software by point counting of 500 individual macerals and determined contents of maceral groups are given in Table 3.

TABLE 3. The determined contents of maceral groups of Nariin sukhait coal.

Sample	Vitrinite Reflectance,	Maceral composition,			
	Ro,%	Vitrinite, %	Liptinite, %	Inertinite,%	Minerals,
Nariin sukhait coal	0,78	70,0	3,0	25,0	2,0

The dates in Table 3 show that the vitrinite's maceral groups have highest content, inertinites middle content and liptinites and minerals have lowest contens of maceral groups in the polished Nariin sukhait coal.

The white-black and collored petrographic photographs are presented in Figure 2.

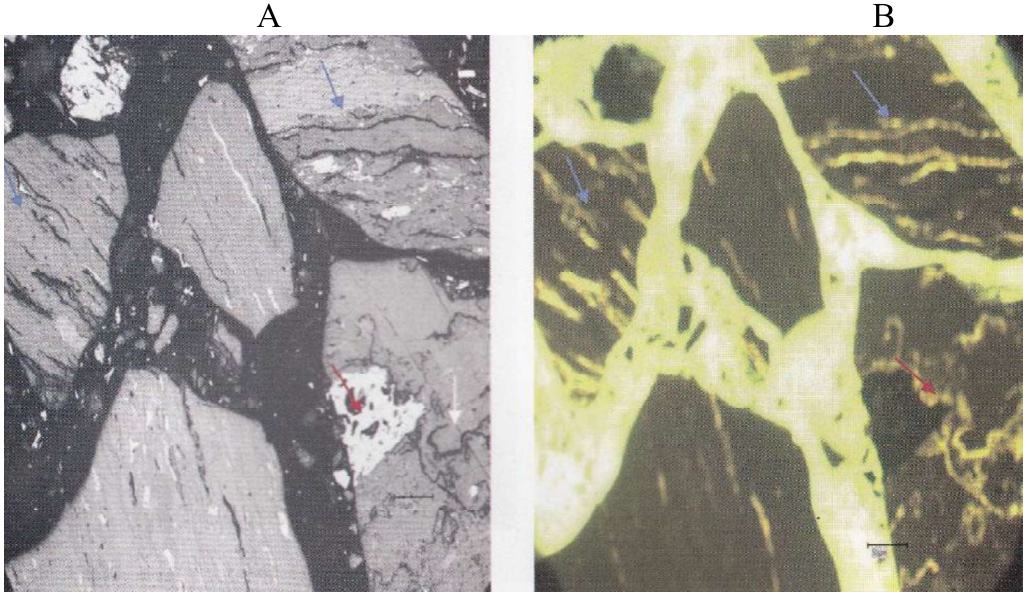

FIGURE 2.The black-white (A) and coloured (B) petrographic photographs of polished coal sample of Nariin sukhait deposit.

The vitrinites are grey coloured fragments with different sizes and the inertinites are white coloured stripes in black-white photograph (Figure 2A). But the liptinites are not observed in black-white photograph (Figure 2A) and they are yellow coloured stripes in coloured photograph (Figure 2B). The vitrinite's fragments are black coloured photograph (Figure 2B). The polymeric (epoxide) binder is a black coloured background in the black-white photograph (Figure 2A) and a green coloured background in the coloured photograph

(Figure 2B). The minerals in the polished coal sample are observed as a brilliant pieces in the microscopy, but they are absent in black-white (A) and coloured petrographic photographs (B).

The degree of vitrinite reflectance (0,78%) was measured using an Axio Imager M2m microscope and Fossil software on 50 individual vitrinite macerals in random mode and the results of measurement is given in Figure 3.

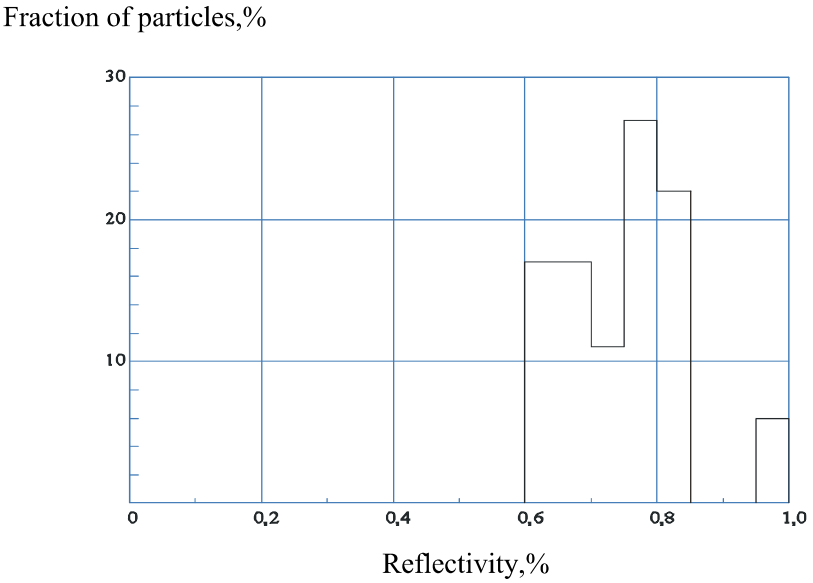

FIGURE 3.Reflectogram of the reflectivity of the vitrinite particles of Nariin sukhait polished coal.

This value 0,78% is characteristic for a high rank G mark bituminous stone coal which is suitable for thermal processing such as coking.

For the investigation of inorganic matter of Nariin sukhait coal the initial coal sample was burned completely and the ash was analyzed by IR (Figure 4) and rentgenfluorecence analysis and determined the chemical composition for the characterization of inorganic matter of the coal from Nariin sukhait deposit and the results are shown in Figure 4 and Table 4.

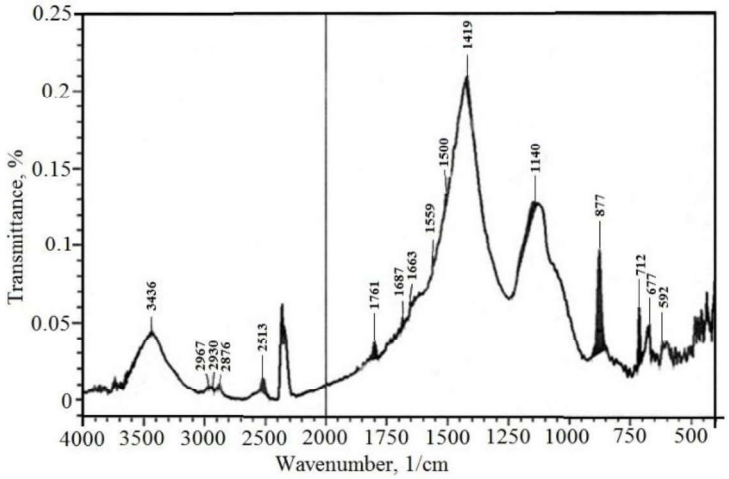

FIGURE 4. The IR spectra of the ash of Nariin sukhait coal.

In the IR spectra (Figure 4) ash of Nariin sukhait coal there is a big absorption band with highest intensity at 1419 cm^{-1} for carbonates – CO_3 for example $CaCO_3$ and $MgCO_3$ and a band with higher intensity for O-Si-O and Si-O-Si groups. A broad band with higher intensity at 3436 cm^{-1} for –OH groups and also a shurp band at 877 cm^{-1} for Al-O- group. There are several peaks with lowest intensity at 712 cm^{-1} for Fe-O- ; at 677 cm^{-1} for Fe-O-Fe and at 592 cm^{-1} for –O-Si-O- groups [5].

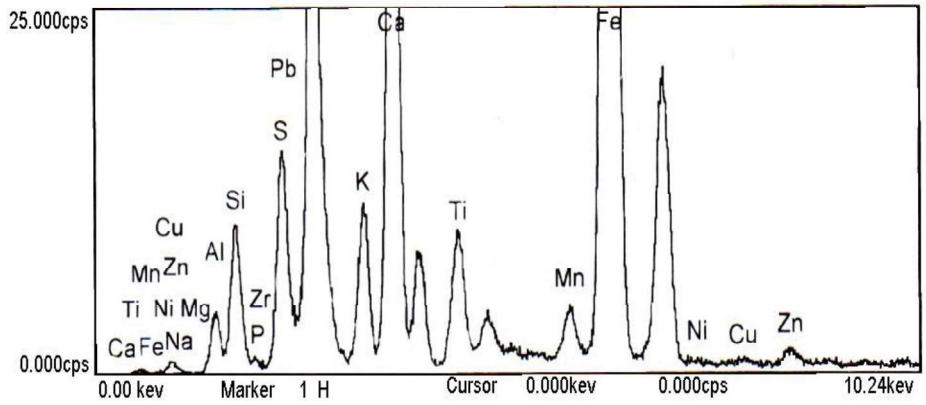

FIGURE 5. Main inorganic elements of Narynsukhait coal element in ash

TABLE 4. Main inorganic elements of Narynsukhait coal oxide in ash, %

Na_2O	MgO	Al_2O_3	SiO_2	P_2O_5	SO_3	K_2O	CaO	Mn_2O_3	Fe_2O_3	TiO_2	SrO	CuO	PbO
1,13	1,47	19,4	25,02	0,40	7,30	1,1	6,30	0,60	7,3	2,70	0,08	0,07	0,09

As seen in the Table 4, there are oxides of Al_2O_3 and SiO_2 have highest concentrations, oxides of CaO, SO_3 ,Fe_2O_3 and TiO_2 have medium concentrations and other oxides have low concentrations. To determine the character (acidic or basic) of the coal was calculated the ratio between following sum oxides: *$(Fe_2O_3+CaO+MgO+Na_2O+K_2O/SiO_2+Al_2O_3+TiO_2)< 0,36$ and if* the ration is less than 1 and it means the coal ash of *Nariin sukhait* deposit has a acidic character.
Also the ash of Nariin sukhait coal was analysed by XRD analysis and the results are given in Figure 6.

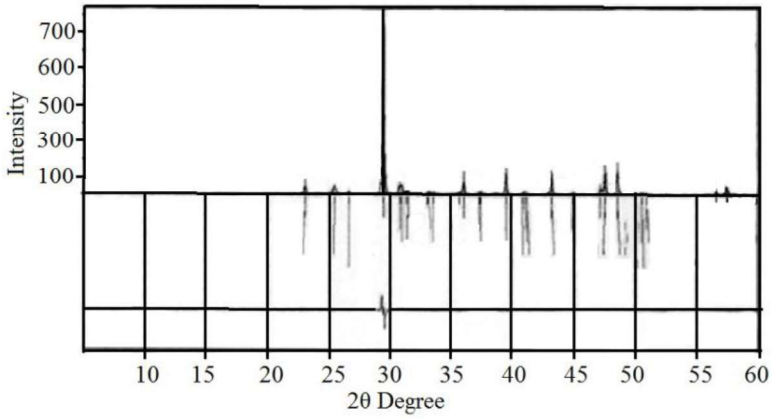

FIGURE 6. Most of the minerals determined in Nariin sukhait coal ash by XRD analysis

The XRD analysis of Nariin sukhait coal ash in Figure 6 show that the ash consists of mainly calcium carbonate $CaCO_3$, acermanit $Ca_2(Mg_{0.75}Al_{0.25})(S_{4.75}Al_{0.25})O_7$, dolomit $CaMg(CO_3)_2$, calcium sulphate $CaSO_4$, and quarz SiO_2.

The contents of radio active elements in the coal and it's ash of *Nariin sukhait coal* determined by Gammaspectrometric analysis and the results are given in Table 5.

TABLE 5. The contents of radio active elements in the coal and it's ash of Nariin sukhait coal.

Sample	Isotop activity, Вк/кg				The content of radio active element			Radium equivalent activity,
	Ra-2	Th-232	K-40	Cs-137	U, g/ton	Th,g/ton	K,%	Ra-Bk/kg
Nariin sukhait coal	8,0	<1,3	<29,4	<1,1	0,7	<0,3	<0,1	5,5
Nariin sukhait coal ash	67,0	26,0	130	<1,1	5,5	6,3	0,4	110,2

The contents of radio active elements in the analytical coal sample Nariin sukhait deposit in Table 5 are lower, but their contents in it's ash increased (enriched) significanty for example the content of U 8 times, Th 21 times and Ra 20 times increased in comparison with initial coal sample.

The thermogravimetric analysis is a most useful method for the investigation on thermal decomposition (in argon atmosphere Hitachi, TG/DTA7300) and thermal stability of natural organic resources including coals.

The thermal decomposition of Nariin sukhait coal in argon gas was investigated by thermogravimetric analyzer in 20 – 1100 °C heating temperatures at heating rates of 20 °C/min. and the TG, DTA and DTG curves are shown in Figure 7.

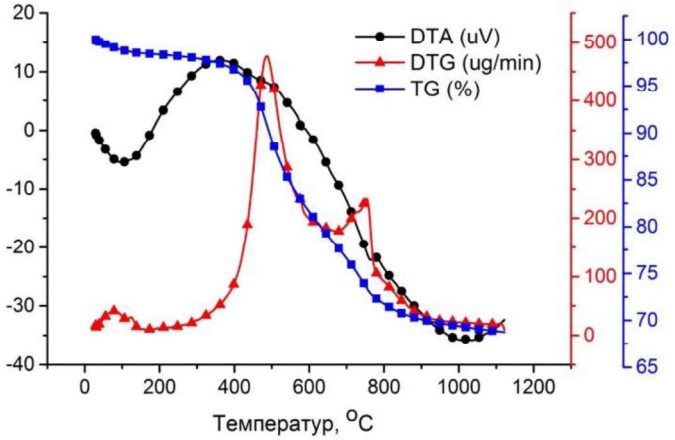

FIGURE 7.TG, DTA and DTG curves of Nariin sukhait coal in argon.

The heating of the Nariin sukhait coal sample at temperatures range 25-1100 °C in argon atmosphere show that the thermal decomposition of coal ended with a 33% weight loss and 67% hard residue at 1100 °C (Figure 7). The TG curve in Figure 7 consists of different temperature intervals (steps) such as 25-425; 425-825; 825-1100 °C. In the first

step (25-425 °C) the weight loss is due to the release of some absorbed gas and moisture from the coal sample. In the second step (425-825 °C) intensive thermal decomposition of the organic matter of the coal samples start forming liquid (tar and pyrolysis water) and gas products. In the third step (825-1100 °C) the weight loss strongly decreases, which is an indication for ending the thermal decomposition and starting carbonization of the coal sample.

From the TG curve in Figure 7 have been determined the thermal stability indices ($T_{5\%}$, $T_{15\%}$, $T_{25\%}$) of the Nariin sukhait coal and compared with the same thermal indices of Shivee-Ovoo brown coal and the results are given in Table 6.

TABLE 6.The the thermal stability indices of the Nariin sukhait and Shivee-Ovoo coals

No	Sample	Thermal stability indices, °C		
		$T_{5\%}$	$T_{15\%}$	$T_{25\%}$
1.	Nariin sukhait coal	425,30	498,6	620,0
2.	Shivee-Ovoo coal	67,5	308,8	465,2

The determined thermal stability indices indicate that the organic mass of Nariin sukhait coal has a much higher thermal stability or is not easy decomposes under heating. For example $T_{5\%}$ of Nariin sukhait coal is more than 6 times higher than that of Shivee-Ovoo brown coal and also $T_{15\%}$ and $T_{25\%}$ of Nariin sukhait coal much higher than that of Shivee-Ovoo brown coal.

First minimum peak of DTA at 160 °C shows a endothermic reaction process related with releasing adsorbed gas and moisture from the coal organic mass of the sample. And a bid exothermic reaction peak at 400 °C related with intensive thermal destruction of the organic mass of the coal sample.

The DTG curves in Figure 7 consist of 2 big zones at 500 °C an 780 °C and and a little zone at 90 °C. The maximum peak happened at 500 °C indicate clearly intensive increasing the thermal decomposition rate of coal organic mass is increasing of heating temperatures. The second maximum peak at 780 °C belongs to relasing of some gas products such as CO; CO_2; H_2; H_2S; NH_3 so on from the carbonized coal residue with lower rate of thermal decomposition. A little maximum paek at 90 °C related with releasing of moisture and adsorbed gases from the coal organic mass with lowest rate of decreasing the weight of coal sample.

The pyrolysis is a one of the often used thermal processing of coals to produce a solid (hard residue or char), condensed liquid (tar) and uncondensed gas product. For this reason the Nariin sukhait coal was pyrolized in a standard quartz retort at different heating temperatures (200°C - 800°C) for 80 min. and determined the yields of char, tar, pyrolysis water and gas (Table 7).

TABLE 7.The yields of pyrolysis products at different heating temperatures.

Sample	Heating temperatures, °C	The yields of pyrolysis products, (%)			
		Hard residue	Tar	Pyrolysis water	Gas and loss
Nariin sukhait coal	200	99.25	-	0.25	0.5
	300	97.86	0.3	1.09	0.75
	400	95.32	0.73	2.47	1.48
	500	92.98	1.05	3.5	2.47
	600	88.53	2.4	4	5.07
	700	83.79	3.66	6.5	6.05
	800	85,33	3,5	5,10	6,10

The results of the pyrolysis of Nariin sukhait coal in Table 7 show that the optimal heating temperature is 700 °C, in which the yield of hard residue and tar (most important products of the pyrolysis) are higher. The yield of all thermal decomposition products such as liquid and gas products (16,0%) shows that there is a thermal decomposition of the coal organic mass with lower degree of conversion. As it is known that the organic mass of high rank coal characterizes with above mentioned higher thermal stability and therefore of high rank coal Nariin sukhait coal is not very suitable for gasification and liquefaction and it more suitable for coking for production of coke with highest yield –about 84,0%.

The solid product (hard residue) with porosity structure after the pyrolysis of Nariin sukhait coal is one of the main product and can be used as coke, smokeless fuel and activated carbon after activation. For this reason have determined the main technical characteristics of the hard residue and compared with the same characteristics of the initial coal (Table 8).

TABLE 8. Main technical characteristics of the pyrolysis hard residue and initial coal of Nariin sukhait deposit.

Nariin sukhait coal	Moisture, W^a	Ash, A^d	Volatile matter, V^{daf}
Initial coal	1.0	15.8	36.9
Hard residue	0.6	17.5	2.8

The volatile matter of the hard residue after pyrolysis decreased more than 13 times, which is a characteristic for intensive removing of the thermal decomposition products from the hard residue during the pyrolysis of Nariin sukhait coal.

One of the most important applications of the hard residue after thermal processing is to produce activated carbon. For this reason the hard residue produced after pyrolysis was activated by preheated water steam at 800 °C for different time (min.) of activation and determined some properties such as iodine adsorption and surface area of the samples (Table 9).

The SEM images of scanning electron microscopes of prepared activated carbon from pyrolyzed hard residue of Nariin sukhait coal (B) in comparison with it's initial coal sample (A) are presented in Figure 8.

TABLE 9. Properties of the activated carbons obtained at temperature 800 °C

No	Sample: Nariin sukhait coal	Time of activation at 800°C, Min.	Iodine adsorption, Mg/g	Iodine number, %	Surface area, (N_2,77K) M^2/g
1	Pyrolysis hard residue	-	4	1,3	-
2	Activated pyrolysis hard residue	60	5	1,6	18
3	Activated pyrolysis hard residue	140	86	27,2	133
4	Activated pyrolysis hard residue	180	420	60,7	402

The dates in Table 9 show that the iodine adsorption and surface area intensively increace is time of activation and reached the best results in time of activation180 min. at 800 °C.

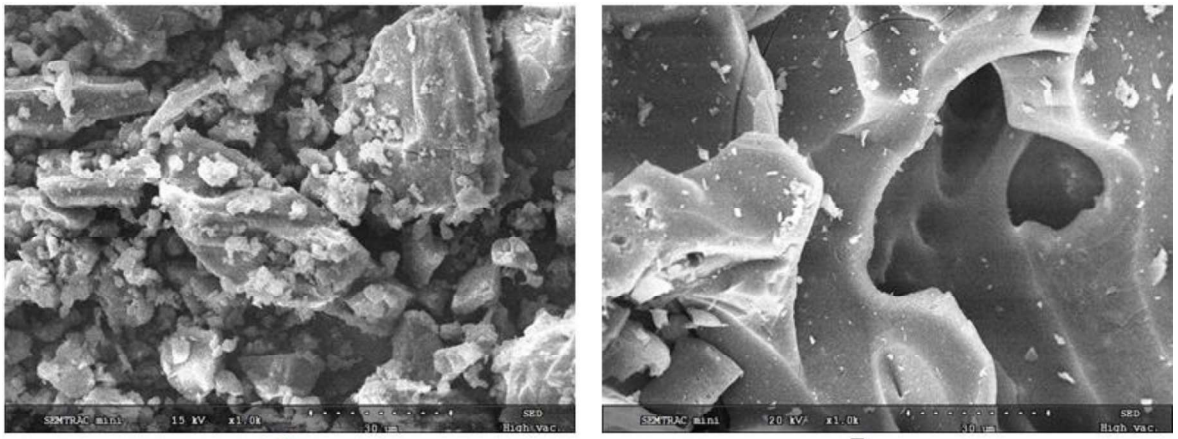

A B

FIGURE 8. SEM microphotographs of activated carbon
(Nariin sukhait coal -A, Nariin sukhait activated carbon –B)

Activated carbon obtained from Nariin sukhait coal by physical activation with preheated water steam has highest iodine adsorption capacity (60.7%) and surface area (402 m^2/g). These values were also comparable with commercial activated carbons obtained from wood (BAU-A carbons data used in Alcoholic and Wine Industries according to Russian standard GOST 6217-74; iodine adsorption capacity (60%). Most suitable condition for the physical activation with preheated water steam was determined as optimal heating temperature 800 °C and time of activation 180 minutes.

The SEM photographic images show that Nariin sukhait initial coal is hard pieces with some micro pores, but the activated carbon sample has a high developed porous material with macro pores mainly after physical activation of cabonized (pyrolized hard residue) Nariin sukhait coal with preheated water steam.

As it was mentioned above the pyrolysis tar of Nariin sukhait coal is also important product with complex properties and composition. Therefore we focused on more detailed investigation of this tar. First of all the tar was completely removed from the pyrolysis water by , centrifuging and drying with thermally treated calcium chloride and filtering. So purified tar was tested for analysis of some technical characteristics such as determination of specific gravity, flamable temperature and combustion temperature (Table 10) and by IR analysis (Figure 9).

TABLE 10. Some technical properties of pyrolysis tar of Nariin sukhait coal

Sample	Specific gravity, g/см^3	Flamable temperature, °C	Combustion temperarure, °C
Pyrolysis tar of Nariin sukhait coal	1,042	69	148

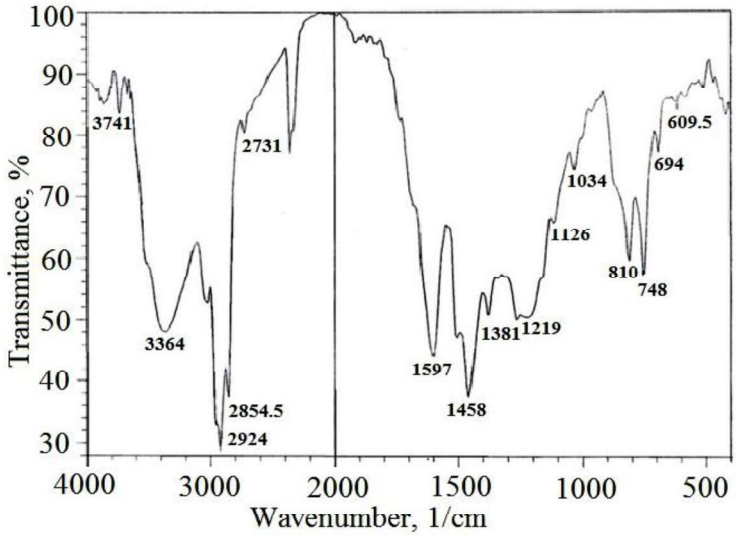

FIGURE 9. The FTIR spectra of liquid tar product after pyrolysis

In the FTIR spectra (Figure 9) of tar product after pyrolysis of Nariin sukhait coal, higher intensity absorption bands were observed for H of aromatic -CH group at 748 and 810 cm^{-1}. A unshurp band with lower intensity for H of aliphatic -CH; -CH_2 and –CH_3 groups at 1218 cm-^{1} and their sharp bands with highest intensity at 2854-2923 cm^{-1}. Absorption bands with higher intensity for O containing groups such as for >C=O groups at 1596 cm^{-1}, for -O- groups at 1458 cm^{-1} and for –O-H groups at 3363 cm^{-1} . Therefore the tar product of Nariin sukhait coal after pyrolysis consists of mainly aliphatic, aromatic and aromatic-aliphatic compounds with above mentioned functional groups in the molecules.

The purified pyrolysis tar of Nariin sukhait coal was tested by an air distillation and obtained several fractions with different boiling temperature ranges and the the yield and some other determined properties are given in Table 11.

TABLE 11. The yields distilled fractions of pyrolysis tar of Nariin sukhait coal

Boiling temperature range , °C	Yield fraction, %	Refractive index	Specific gravity, g/cm^3	Color	Description
Startin loiling -180 °C	4,7	1,455	0,71	yellow	light fraction
180-250 °C	11,7	1,519	0,89	yellow-green	middle fraction
250-320 °C	9,0	1,532	0,89	brown	middle fraction
< 320 °C	59,90	-	-	black	heavy fraction

The date in Table 11 show that the main product of distillation of the pyrolysis tar of Nariin sukhait coal is the heavy fractions, followed light and middle fractions with same yields. After removing of the toxic organic compounds such as organic bases, organic acids and phenols these fractions can be used as gasoline (light fractions), diesel (middle fractions) and oil products (heavy fractions).
The chemical composition of the tar determined by chemical analysis in group organic compounds and the results are given in Table 12.

TABLE 12. The chemical composition of the tar in group organic compounds

Sample	The chemical composition of the tar , мas. %					
	free carbons	organic bases	organic acids	phenols	asphalteins	neutral oils
pyrolysis tar of Nariin sukhait coal	2,6	1,0	5,5	3,4	2,5	85,0

The date in Table 12 show that the neutral oils are the main component with highest and asphalteins, free carbons, phenols and organic acids are with middle content. The content of organic bases has lowest content.

As mentioned above organic bases and organic acids were removed from the pyrolysis tar of Nariin sukhait coal and so purified tar is called as a ''neutral oil''.

The purified tar was subjected on a silicagel chromotagraphy and eluted by hecsane (H), benzene (B) and dichloromethane (M) in consecutive order and the yields of fractions determined (Table 13).

TABLE 13. The yields of fractions soluble in hecsane (H), benzene (B) and dichloromethane (M) of the pyrolysis tar of Nariin sukhait coal.

Nariin sukhait coal	Analytical sample of tar		Hexane (H) soluble fraction		Benzene (B) soluble fraction		Dichloromethane (M) soluble fraction		All isolated samples	
	g.	%	g.	%	g.	%	g.	%	g.	%
Tar	0,25	100,0	0,0859	34,36	0,05	20,0	0,0232	9,3	0,1591	63,66

The dates of solublity of the pyrolysis tar of Nariin sukhait coal in Table 9 show that the hexane (H) soluble fraction has highest content (34.36%), the benzene (B) soluble fraction has middle content (20,00%) and the dichloromethane (M) soluble fraction has lowest content (9,30%).

Each of these 3 fractions were analized by GC/MS analysis for determination of the chemical composition of every fraction of the pyrolysis tar of Nariin sukhait coal and the chromatograms are presented in Figure 10 (H), 11(B) and 12 (M)..

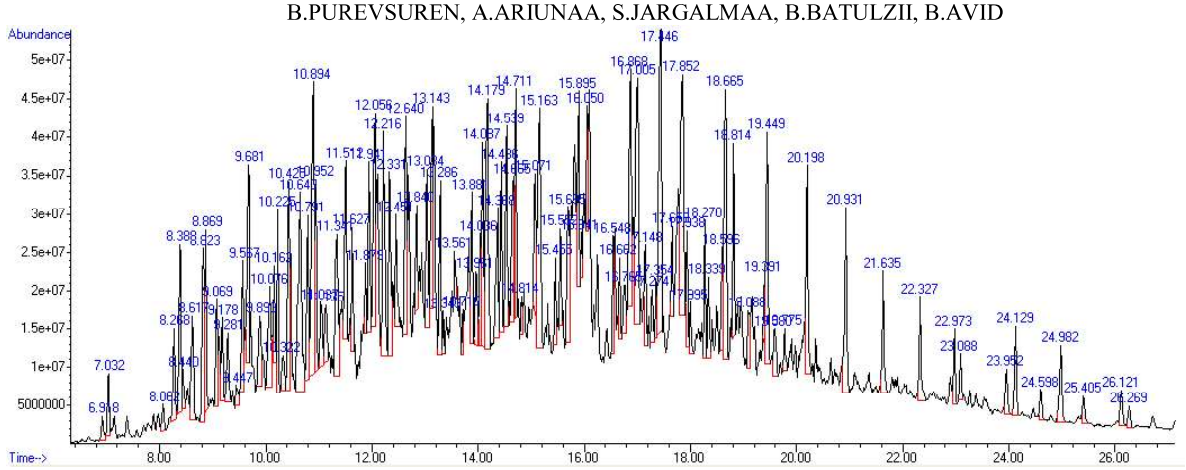

Elution time, min.

FIGURE 10. GC/MS chromatogram of soluble in hexane fraction of the the pyrolysis tar of Nariin sukhait coal.

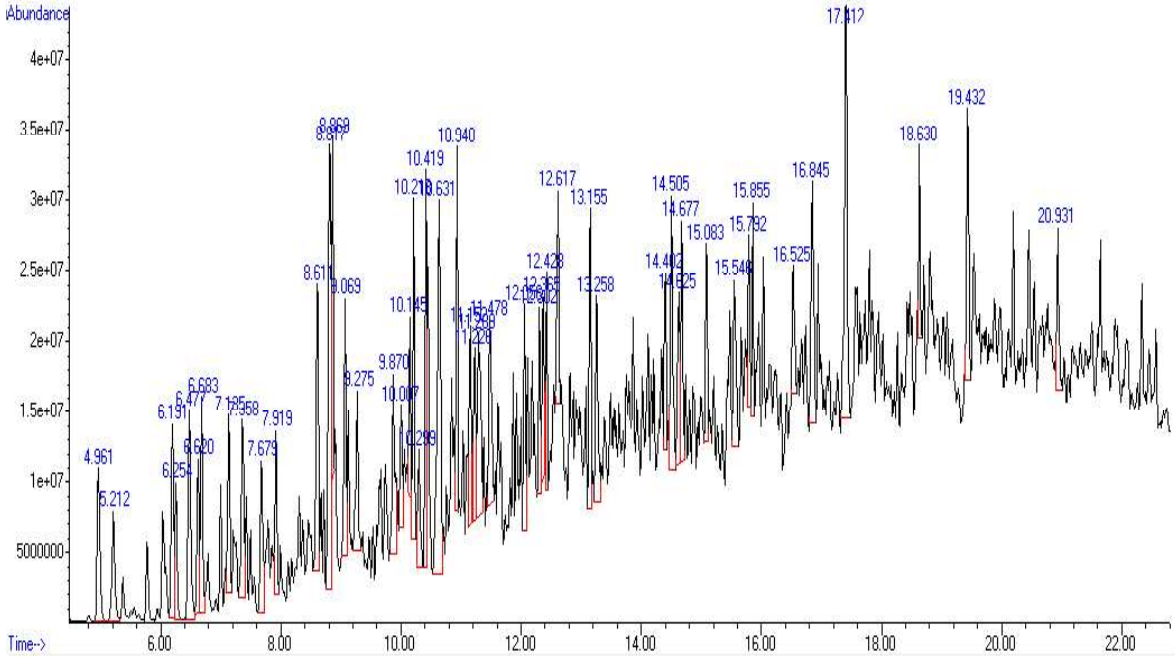

Elution time, min.

FIGURE 11.GC/MS chromatogram of soluble in benzene fraction of the pyrolysis tar of Nariin sukhait coal.

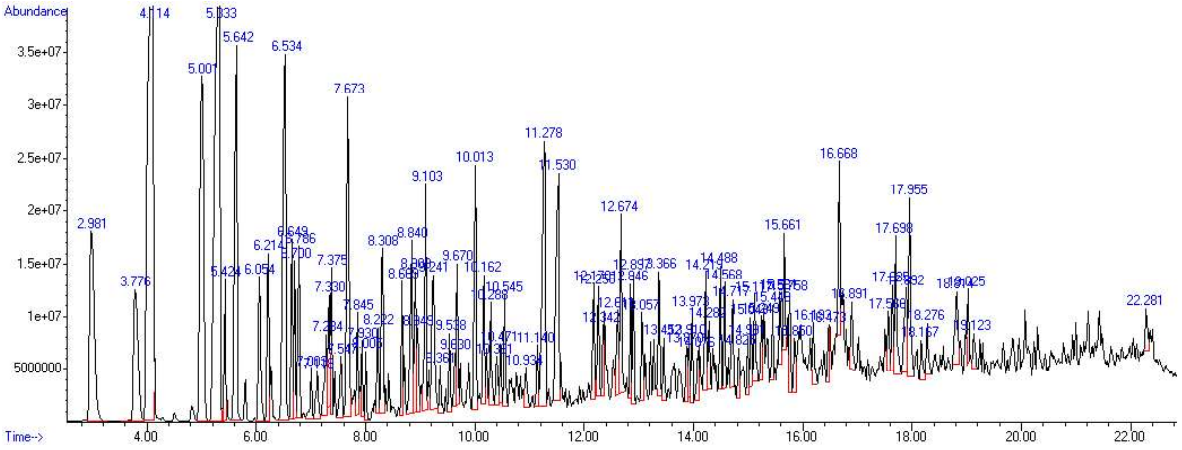

Elution time, min.

FIGURE 12. GC/MS chromatogram of soluble in dichloromethane fraction of the the pyrolysis tar of Nariin sukhait coal.

All 41 compounds identified from all registered 100 peaks of soluble in hexane (Figure 10), 35 compounds identified from all registered 50 peaks of soluble in benzene (Figure 11), and 19 compounds identified from all registered 91 peaks of soluble in dichloromethane (Figure 12) in the pyrolysis tar of Nariin sukhait coal.

The pyrolysis tar were separated by column chromatography and analyzed by GC/MS. Results are shown in Table 13. The yield of aliphatic fraction was 34.4 wt%, aromatic fraction 20.0 wt%, polar fraction 9.3 wt% of pyrolysis tar. The tar product from coal contained aliphatic, aromatic hydrocarbon, phenol, with higher polycyclic aromatic hydrocarbon and alkylphenols. Aliphatic and aromatic fractions contain high amounts of hydrocarbons. Total amount of hydrocarbons were 67.5 wt%, 54.7 wt% in aliphatic and aromatic fractions respectively. Polar fraction contains 32.2 wt% one and two ring phenols.

TABLE 13. Composition of pyrolysis tar by column chromatography and GC/MS

Aliphatic fraction (total 34.4), %		Aromatic fraction (total 20.0), %		Polar fraction (total 9.3), %	
aliphatic	34.1	one and two ring aromatics	37.2	phenolic compounds	26.7
aromatic	33.4	three ring aromatics	17.5	two ring phenolic compounds	5.5
others	32.5	others	45.3	others	67.8

4. CONCLUSIONS

1. On the basis of proximate, ultimate and petrographic analysis have been confirmed that the Nariin sukhait coal is a high-rank bituminouce coal of G mark and it is suitable for thermal processing including coking and activation.
2. The thermal degradation process of Nariin sukhait coal was investigated by thermogravimetric analyzer and first time determined the thermal stability of the coal sample by determination of thermal indices such as $T_{5\%}$ -425,3°C; $T_{15\%}$ -498,6°C; $T_{25\%}$ - 620,0°C from the TG curve, which are the characteristics of higher thermal stability of the coal organic mass.
3. The results of pyrolysis experiment of Nariin sukhait coal show that about 84,0% of coal organic mass remained as a hard residue after pyrolysis. The yield of all liquid and gas products is 16,0% at the optimal heating temperature 700°C, which is showing that there was a thermal decomposition of the coal organic mass with lower degree of conversion and higher degree of coking.
4. The determined chemical composition of pyrolysis tar of Nariin sukhait coal in group organic compounds by chemical analysis show that the tar consists mostly neutral oils with highest content-85,0%, asphalteines -13,6%, organic acids and phenolic compounds are with lower content, organic bases and asphalteins are with lowest content.
5. The pyrolysis tar of Nariin sukhait coal also was distilled at room temperature and obtained 4 fractions with different boiling temperature ranges including yellow colored light fraction (18-180°C), 2 yellow-green colored middle fractions (180-250 °C and 250-320 °C) and black colored heavy fraction (330 >°C).
6. The SEM image of initial coal sample Nariin sukhait has compact solid pieces. SEM image of carbonized and activated coal sample shows a porosity structure with meso and macro pores in comparison with that of initial coal sample.
7. The solubility in hecsane, benzene and dichloromethane and chemical composition of the pyrolysis tar of Nariin sukhait coal investigated by silicagel chromatograpy and chemical composition of the each separated fractions determined by GC/MS analysis. All 41 compounds identified from all registered 100 peaks of soluble in hexane, 35 compounds identified from all registered 50 peaks of soluble in benzene , and 19 compounds identified from all registered 91 peaks of soluble in dichloromethane in the pyrolysis tar of Nariin sukhait coal

REFERENCE

[1] P.Ochirbat et al.*Coal Industry of Mongolia in XX centure,* Book, 2002, p.29-30.
[2] B.Avid, *Chemistry and Technology of Coal*, Monograph, Publisher ''Bindzor ''2018, p.11.
[3] B.Purevsuren, Ya.Davaajav, R.Erdenechimeg, *Investigation of coals of some big deposits in Mongolia*, Monograph, Publisher ''Toonot Print'', 2010, p.88-112.
[4] Ya.Davaajav, B.Purevsuren, *Petrographical study of coals of some Mongolian deposits*, Monograph, Publisher ''Toonot Print',2016, p.166-177.
[5] I.I.Plusnina, *Infra Red Spectra of Minerals*, Book, Publisher ''Moscow University'', 1977, p.50-51, 57, 103,109.

OPTIWIM – OPTIMIZATION OF THE RECOVERY OF CRITICAL MINERAL RESOURCES FROM POLYMETALLIC ORE DEPOSITS

MEYER FM[1/3], BAUER M[4], BYAMBA E[4], GRONEN L[1], HELLMANN A[1], KATZMARZYK J[2], SINDERN S[1], WEYER T[4], WOTRUBA H[2]

[1]INSTITUTE OF APPLIED MINERALOGY AND ECONOMIC GEOLOGY, RWTH AACHEN UNIVERSITY, WÜLLNERSTR. 2, 52062 AACHEN, GERMANY

[2]UNIT OF MINERAL PROCESSING (AMR), RWTH AACHEN UNIVERSITY, LOCHNERSTRAßE 4-20, 52064 AACHEN, GERMANY,

[3]GERMAN-MONGOLIAN INSTITUTE OF RESOURCE TECHNOLOGY, GMIT CAMPUS, 2ND KHOR, NALAIKH DISTRICT, ULAANBAATAR, MONGOLIA

[4]GESELLSCHAFT FÜR CONSULTING, BUSINESS UND MANAGEMENT (CBM GMBH) NIEDERBEXBACHER STRASSE 67, 66450 BEXBACH, GERMANYMONGOLIA

E-mail address: m.meyer@rwth-aachen.de

ABSTRACT. OptiWiM is a private-public-partnership (ppp) program involving the mining consultant company CBM and two RWTH Aachen University departments. Financial support is provided by the German Federal Ministry of Education and Research (BMBF). Collaborative Mongolian partners are the Germany Mongolian Institute of Resources Technology (GMIT), MONNIS International LLC, and the TD Bank of Mongolia.

The OptiWiM study integrates sophisticated mining design, sequential mineral beneficiation tech¬niques, and automated quantitative process mineralogy to avoid the predicted exhaustion of critical mineral commodities demanded by high-tech industries.

Critical minerals are metals that are central to high-technology sectors, whereby criticality is determined by the vulnerability to supply disruption and the economic importance to industry. In many cases, critical elements are geologically dispersed, concentrated in a few geographic locations or recovered as a byproduct of another commodity.

Polymetallic ores, by nature, contain a complex and diverse mineral assemblage, which requires special beneficiation strategies to become technically and economically feasible. Alkaline granitoid rocks are often significantly enriched in high-tech metals such as the REE, Y, Nb or Zr, but most of the associated ore bodies are currently not being exploited for economic reasons. This is mainly because of their pronounced mineralogic and textural heterogeneity, which, in turn, causes severe difficulties in ore processing. On the other hand, mining of critical metals as by-product of major commodities has a significant economic advantage since extraction costs are shared by the bundle of metals mined.

The OptiWiM study focusses on the Alkaline massif of Khalzan Buregtei in western Mongolia. Automated process mineralogy is employed to determined parameters such as mineral abundance, mineral intergrows, grain size distribution, and chemical composition of the ore. This information is essential for the selection of the most sustainable and efficient mineral beneficiation process. The distribution of ore and gangue minerals serves

as basis for computer-aided 3D models used for the design of the most suitable extraction process.

Results indicate that mineral textures and assemblages are obscured by a post-magmatic hydrothermal overprint by an Fe-rich fluid phase which initiated Zr- and REE-bearingore minerals to form hematite-cemented mineral clusters of grain sizes up to 250 µm. This allows a pre-concentration of the ore mineral clusters by magmatic separation following less energy consuming comminution to particle sizes < 250 µm. The study has as its underlying premise that a joint geometallurgical, mineral processing and mineral extraction approach is needed to become proficient in delivering a suite of critical elements from polymetallic ores. The design of efficient mining and processing techniques for such ores augments the quest for higher resource efficiency.

GENERALIZED SOLUTIONS OF INTEGRO-DIFFERENTIAL EQUATIONS OF THE VISCOELASTICITY THEORY

FALALEEV M.V.

INSTITUTE OF MATHEMATICS, ECONOMICS AND INFORMATICS, IRKUTSK STATE UNIVERSITY, IRKUTSK, 664003, RUSSIA

Email address: mvfalaleev@gmail.com

ABSTRACT. The initial-boundary value problems for the integro-differential equations of the theory of viscoelasticity are considered in terms of the theory of fundamental operator functions for the degenerate equations in Banach spaces.

1. INTRODUCTION

Let us consider analogs of the initial-boundary value problems from the theory of viscoelasticity [1] for degenerate equations.

$$(\lambda - \Delta)\, u_{tt} - (\mu - \Delta)\, u - \int\limits_0^t g(t-\tau)\Delta^2 u(\tau, \bar{x})d\tau = f(t, \bar{x}), \tag{1}$$

or

$$(\lambda - \Delta)\, u_{tt} - (\mu - \Delta)\, u - \int\limits_0^t g(t-\tau)\left(\lambda^2 - \Delta^2\right) u(\tau, \bar{x})d\tau = f(t, \bar{x}), \tag{2}$$

with conditions

$$u\Big|_{t=0} = u_0(\bar{x}), \;\; u_t\Big|_{t=0} = u_1(\bar{x}), \;\; \bar{x} \in \Omega; \;\; u\Big|_{\bar{x}\in\partial\Omega} = 0, \;\; t \geq 0, \tag{3}$$

where $g(t),\;\; f(t, \bar{x})$ are the functions given; $u = u(t, \bar{x})$ is the unknown function; $\bar{x} \in \Omega \subset R^m$ is a bounded domain with an infinitely smooth boundary $\partial\Omega;\;\; \Delta$ the Laplace operator; and $u = u(t, \bar{x})$ is defined on the cylinder $R_+ \times \Omega,\;\; \lambda \in \sigma(\Delta)$.

These problems, being represented in the abstract form, can be reduced to degenerate integro-differential equations in the Banach spaces.

Let us consider the following initial-value problem of the form

$$Bu^{(N)}(t) = Au(t) + \int_0^t K(t-s)u(s)ds + f(t), \tag{4}$$

$$u(0) = u_0,\; u'(0) = u_1,\; \ldots,\; u^{(N-1)}(0) = u_{N-1}, \tag{5}$$

Key words and phrases. Banach spaces, Fredholm operator, generalized function, fundamental solution.

where $B; A; K(t)$ are closed linear operators with dense domains acting from E_1 to E_2; E_1 and E_2 are the Banach spaces, B is a Fredholm operator (see [2]), and $f(t)$ is a sufficiently smooth function with values in E_2.

Next, for (4)-(5), let us assume that $D(B) \subset D(A)$; $D(K(t)) = D(K) \subset D(B)$ and $D(K)$ is independent of t; $\overline{D(A)} = \overline{D(B)} = \overline{D(K)} = E_1$; $\overline{R(B)} = R(B)$; $\dim N(B) = \dim N(B^*) = n \geq 1$.

2. Auxiliary designations and information

Let $\{\varphi_i\} \in E_1$ be a basis of the kernel for operator B; $\{\psi_i\} \in E_2^*$ be a basis of the kernel for adjoint operator B^*; $i = 1, \ldots, n$ and $\{z_i\} \in E_2$, and $\{\gamma_i\} \in E_1^*$ be the corresponding biorthogonal systems of elements. In this case (see [2]), there exists a bounded Trenogin-Schmidt operator of the form

$$\Gamma = \left(B + \sum_{i=1}^{n} \langle \cdot, \gamma_i \rangle z_i \right)^{-1} \in L(E_2, E_1).$$

Let us introduce the following conditions.

A) there exists a complete A-Jordan set $\left\{ \varphi_i^{(j)} \right\} \in E_1$ of the operator B and a complete A^*-Jordan set $\left\{ \psi_i^{(j)} \right\} \in E_2^*$ of the operator B^*, $i = 1, \ldots, n$, $j = 1, \ldots, p_i$; elements of the sets (adjoint elements) may be restored in accordance with the rules $\varphi_i^{(j)} = (\Gamma A)^{j-1} \varphi_i$, $\psi_i^{(j)} = (\Gamma^* A^*)^{j-1} \psi_i$ (see [2] for the rest of information and for more complete information about the adjoint elements, in particular, if there exists $\epsilon > 0$ such that for all $0 < |\lambda| < \epsilon$, $\exists\ (B - \lambda A)^{-1} \in L(E_2, E_1)$, then condition **A)** is satisfied), $p = \max p_i$.

B) the operator-valued function $K(t)$ is sufficiently smooth, furthermore, either

B1) $K^{(\nu)}(0) = 0, \ \ \nu = 0, 1, \ldots, N \cdot (p-1) - 1, \ p > 1;$

or

B2) $\varphi_i^{(j)} \in N(K^{(\nu)}(0)), \ \ \nu = 0, 1, \ldots, N \cdot (p-1) - 1, \ p > 1;$

or

B3) $\psi_i^{(j)} \in R^{\perp}(K(t)), \ \ \nu = 0, 1, \ldots, N \cdot (p-1) - 1, \ p > 1;$

or

B4) $\psi_i^{(j)} \in N(K^{*(\nu)}(0)), \ \ \nu = 0, 1, \ldots, N \cdot (p-1) - 1, \ p > 1.$

In terms of conditions A) and B) let us introduce the following denotation:

$$\tilde{Q} = \sum_{i=1}^{n} \sum_{j=1}^{p_i} \langle \cdot, \psi_i^{(j)} \rangle A \varphi_i^{(p_i + 1 - j)},$$

for the projector

$$U_N(A\Gamma t) = \sum_{k=1}^{\infty} (A\Gamma)^{k-1} \frac{t^{kN-1}}{(kN-1)!}$$

of the operator-valued function

$$H(t) = K(t)\theta(t) * \Gamma U_N(A\Gamma t) \left[I - \tilde{Q} \right] \theta(t) -$$

$$-\sum_{i=1}^{n}\left[\sum_{k=0}^{p_i-1}\left\{\sum_{j=1}^{p_i-k}\left\langle\cdot,\psi_i^{(j)}\right\rangle K^{(N\cdot k)}(t)\varphi_i^{(p_i-k+1-j)}\right\}\right]\theta(t),$$

$$\tilde{H}(t)=\Gamma U_N(A\Gamma t)\left[I-\tilde{Q}\right]\theta(t)*K(t)\theta(t)-$$

$$-\sum_{i=1}^{n}\left[\sum_{k=0}^{p_i-1}\left\{\sum_{j=1}^{p_i-k}\left\langle K^{(N\cdot k)}(t)\cdot,\psi_i^{(j)}\right\rangle\varphi_i^{(p_i-k+1-j)}\right\}\right]\theta(t),$$

for the kernels, and for their resolvents $R(t)$ and $\tilde{R}(t)$, respectively.

Under conditions **A)** and **B)**, the initial-value problem (4)-(5) is solvable in the class $C^N(t\geq 0)$ only if the special conditions of relation between the initial conditions (5) and function $f(t)$ hold. Let us construct the generalized solutions of the initial-value problem (4)-(5) in the space of generalized functions (distributions) with left-bounded support (see [3], [4]) with the use of the fundamental operator function for the integro-differential equation (4) of the form $(B\delta^{(N)}(t)-A\delta(t)-K(t)\theta(t))$. If $K(t)\equiv 0$, hence (see [3], [4]) the fundamental operator function for the differential operator $(B\delta^{(N)}(t)-A\delta(t))$ writes:

$$\tilde{E}_N(t)=\Gamma U_N(A\Gamma t)\left[I-\tilde{Q}\right]\theta(t)-\sum_{i=1}^{n}\left[\sum_{k=0}^{p_i-1}\left\{\sum_{j=1}^{p_i-k}\left\langle\cdot,\psi_i^{(j)}\right\rangle\varphi_i^{(p_i-k+1-j)}\right\}\delta^{(N\cdot k)}(t)\right].$$

Due to condition **B)**, the following convolution equalities are valid: $H(t)=K(t)\theta(t)*\tilde{E}_N(t)$, $\tilde{H}(t)=\tilde{E}_N(t)*K(t)\theta(t)$ and $\tilde{E}_N(t)*R(t)=\tilde{R}(t)*\tilde{E}_N(t)$.

3. THEOREMS ON THE FUNDAMENTAL OPERATOR-VALUED FUNCTIONS

The following theorem is valid

Theorem 3.1. *If the conditions* **A)** *and* **B)** *are satisfied, then the integro-differential operator* $(B\delta^{(N)}(t)-A\delta(t)-K(t)\theta(t))$ *has on class* $K'_+(E_1)$ *of distributions with the left-bounded support the fundamental operator-valued function of the form*

$$E_N(t)=\tilde{E}_N(t)*(I\delta(t)+R(t)\theta(t))=(I\delta(t)+\tilde{R}(t)\theta(t))*\tilde{E}_N(t).$$

Under the conditions of Theorem 3.1, the only (unique) generalized solution of the initial-value problem (4)-(5) in the class $K'_+(E_1)$ is represented as a generalized function of the form

$$\tilde{u}(t)=E_N(t)*\left(f(t)\theta(t)+Bu_{N-1}\delta(t)+Bu_{N-2}\delta'(t)+\cdots+Bu_0\delta^{(N-1)}(t)\right),\quad(6)$$

It is possible to obtain the conditions for the solvability of problem (4)-(5)) in the class $C^N(t\geq 0)$ from this representation.

In particular, the following statement may be made.

Theorem 3.2. *If* $N=2$ *in equation (4), and the lengths of all A-Jordan chains are 1, then the initial-value problem (4)-(5) has a unique solution in the class* $C^2(t\geq 0)$ *if and only if the conditions*

$$\langle Au_0+f(0),\psi_i\rangle=0,\ \left\langle Au_1+f'(0)+K(0)u_0,\psi_i\right\rangle=0,\quad i=1,\ldots,n.$$

are satisfied.

Let for the Cauchy-Dirichlet problems (1)-(3) and (2)-(3) $\mu \neq \lambda$, we have

$$E_1 \equiv \left\{v(\bar{x}) \in W_2^4(\Omega) :\ v|_{\partial\Omega} = 0\right\},\ E_2 \equiv W_2(\Omega),\ B = \lambda - \Delta,\ A = \mu - \Delta,\ \ \lambda \in \sigma(\Delta),$$

where $W_2^4(\Omega)$ and $W_2(\Omega)$ are Sobolev spaces; $\varphi_i(\bar{x})\ \ i = 1, \ldots, n$ is a basis of the space of solutions for the homogeneous problem: $\lambda\varphi_i = \Delta\varphi_i,\ \varphi_i|_{\bar{x}\in\partial\Omega} = 0$. Here the lengths of all A-Jordan chains are 1.

Now, using Theorem 3.2 we obtain the following.

Theorem 3.3. *The Cauchy-Dirichlet problem (1)-(3) is uniquely solvable in a class $C^2(t \geq 0)$ if and only if the initial conditions (3) and the function $f(t, \bar{x})$ satisfy the relations*

$$\left\langle (\mu - \lambda)u_1(\bar{x}) + f_t'(0, \bar{x}) + g(0)\lambda^2 u_0(\bar{x}), \varphi_i(\bar{x})\right\rangle = 0,$$
$$\left\langle (\mu - \lambda)u_0(\bar{x}) + f(0, \bar{x}), \varphi_i(\bar{x})\right\rangle = 0, \quad i = 1, \ldots, n,$$

Theorem 3.4. *The Cauchy-Dirichlet problem (2)-(3) is uniquely solvable in a class $C^2(t \geq 0)$ if and only if the initial conditions (3) and the function $f(t, \bar{x})$ satisfy the relations*

$$\left\langle (\mu - \lambda)u_1(\bar{x}) + f_t'(0, \bar{x}), \varphi_i(\bar{x})\right\rangle = 0,\ \left\langle (\mu - \lambda)u_0(\bar{x}) + f(0, \bar{x}), \varphi_i(\bar{x})\right\rangle = 0,\ i = 1, \ldots, n,$$

CONCLUSION

The method proposed in the paper allows one to construct a unique generalized solution corresponding to formula (6). On the basis of analysis of representation (6) it is possible to obtain unique smooth solutions of problem (4)-(5). Abstract results of these theorems may be applied, for example, in the investigation of mathematical models of the theory of oscillations in viscoelastic media or the theory of electric chains.

REFERENCES

[1] M.M. Cavalcanti, V.N. Domingos Cavalcanti and J. Ferreira *Existence and Uniform Decay for a Non-Linear Viscoelastic Equation with Strong Damping*, Math. Meth. Appl. Sci., **24** (2001), 1043–1053.

[2] M.M. Vainderg and V.A. Trenogin *Theory of Branching of Solutions to Nonlinear Equations* [in Russian], Nauka, Moscow (1969).

[3] N. Sidorov, B. Loginov, A. Sinitsyn and M. Falaleev *Lyapunov-Schmidt Methods in Nonlinear Analysis and Applications*, Kluwer Academic Publ., Dordrecht (2002).

[4] M.V. Falaleev *Fundamental Operator-functions of Singular Differential Operators in Banach Spaces*, Sib. Math. J., **41** (2000), 960–973.